

A Modular Architecture Design for Autonomous Driving Racing in Controlled Environments

Brais Fontan-Costas[✉], M. Diaz-Cacho[✉], Ruben Fernandez-Bouillon[✉], Manuel Alonso-Carracedo[✉], Javier Perez-Robles[✉]

Abstract—This paper presents an Autonomous System (AS) architecture for vehicles in a closed circuit. The AS performs precision tasks including computer vision for environment perception, positioning and mapping for accurate localization, path planning for optimal trajectory generation, and control for precise vehicle actuation. Each subsystem operates independently while connecting data through a cohesive pipeline architecture. The system implements a modular design that combines state-of-the-art technologies for real-time autonomous navigation in controlled environments.

I. INTRODUCTION

Autonomous vehicle systems in controlled environments present significant challenges in integrating multiple subsystems for real-time navigation and decision-making. The development of modular architectures that effectively combine perception, localization, path planning, and control systems represents a critical area of research in autonomous driving technology. This work presents a comprehensive framework for the connectivity and allocation of responsibilities within an autonomous driving architecture, focusing on precise operation in closed-circuit scenarios. The approach defines four primary modules: perception, localization and mapping, trajectory planning, and control. It also describes their interconnection through a communication pipeline. The paper also reviews the current state of the art, analyzes the main technological advances, and justifies the design choices made to address the scientific and engineering challenges faced by autonomous vehicles in constrained, competitive or experimental environments.

II. VEHICLE AND HARDWARE ARCHITECTURE

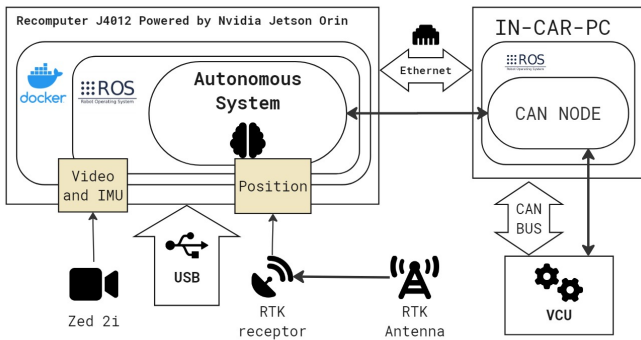


Figure 1. Hardware Architecture

A. Hardware architecture

The dual-computer architecture consists of five primary components: a ZED 2i stereo camera, a simpleRTK2B receiver, a reComputer-based on-board computer (primary autonomous system host), a dedicated in-car PC (secondary computer for CAN communication), and the VCU. The on-board computer executes all perception, planning, and control modules, while the in-car PC handles CAN

Bus communication and ROS interfacing with the Vehicle Control Unit. This separation ensures computationally intensive algorithms run independently from real-time communication interfaces.

B. Hardware Components

1) *On-board computer*: The AS runs on a reComputer J4012 powered by the NVIDIA® Jetson Orin NX module [1]. This System-on-Module (SoM) features an integrated Ampere GPU with 1024 CUDA cores and dual deep learning accelerators, delivering up to 100 TOPS of AI performance for the vision pipeline. The system operates on Ubuntu 20.04 with ROS 2 Galactic, utilizing the architecture described by Macenski et al. [2]. The middleware is virtualized via Docker to ensure compatibility, while the in-car PC runs Ubuntu 22.04 with ROS 2 Humble.

2) *Real-time kinematic positioning*: The simpleRTK2B module from ArduSimple [3] provides centimeter-level GNSS accuracy. It utilizes the u-blox ZED-F9P multiband GNSS engine to receive corrections from a fixed base station up to 11 km away. The rover board computes Real-Time Kinematic (RTK) solutions at a rate of 10 Hz, providing the high-precision absolute positioning required for the Extended Kalman filter updates.

3) *ZED 2i Stereo camera*: The ZED 2i [4] captures 1920x1080 stereo images at 30fps with a 120° field of view. It integrates a 9-DOF IMU (accelerometer, gyroscope, and magnetometer) running at 400 Hz, which is factory-calibrated and synchronized with the video stream. Its IP66-rated enclosure ensures reliability during adverse weather conditions typically encountered in competition.

4) *CAN Bus*: Data transmission between the in-car PC and VCU relies on the Controller Area Network (CAN) protocol [5]. The interface adheres to the specific AS-DV software specification defined for the competition [6], categorizing messages into control commands, sensor feedback, and mission status flags.

III. SOFTWARE

A. Software architecture

The AS is developed on ROS2 [7], a software framework that provides utilities for complex robotic machines. Each module is implemented via a ROS2 package and each submodule is implemented via ROS2 nodes as illustrated in Figure 2.

B. Computer Vision

The main objective of the computer vision module is to take camera images and process them in order to detect the cones that delimit the track. The object detection and depth calculation nodes take left and right images from the camera driver. A computer vision model is used to detect the cones delimiting the track, while a depth calculating algorithm calculates a depth image. Using both the detections and the depth information, the positioning node calculates a bird's eye view positioning of the cones relative to the car. The nodes that are part of the computer vision module are marked in red in the figure 2.

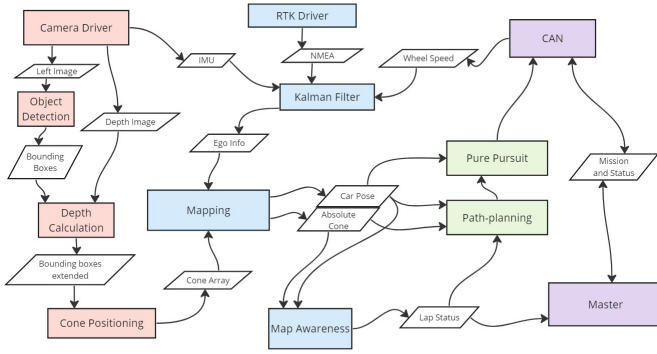


Figure 2. Software Architecture

1) *Depth calculation*: Stereolabs offers as part of their SDK for the ZED a depth calculation functionality [8]. It allows a variety of depth calculation modes, that change the performance and speed of the calculation. During our experiments, the best results were obtained by using the Neural mode. This mode uses an end to end AI powered calculation. This calculation is very computer intensive and uses CUDA to compute the depth in the reComputer.

An analysis of the depth accuracy of this module was done by placing objects at a set distance from the camera and registering the variability of the measured depth. Figure 7 presents the distribution in quartiles of the measurements. The error increases exponentially with distance, reaching a median error of 0.5 meters at an 8 meter distance. It is also noticeable that there are outliers at all measured intervals. The use of a visual tracker, combined with the mapping algorithm mitigates this depth error.

2) *Object Detector*: YOLO is one of the most popular real-time object detectors. Its success can be attributed to the following factors: 1) A lightweight network architecture. 2) Effective feature fusion methods. 3) More accurate detection results. YOLOv11 presented a model that performed better than state-of-the-art models in accuracy and efficiency [9]. The YOLO family of object detection models is focused on balancing speed and accuracy for real time applications.

YOLOv11 [10] was released in September 2024 by Ultralytics [11]. There are some pre-prints that analyse the performance of the YOLOv11 model [12]. In these pre-prints the YOLOv11 model performed better than its predecessors in speed and accuracy. For these reasons, YOLOv11 was chosen as the detection model.

Ultralytics offers different pretrained models to use as training baseline. The YOLOv11 model chosen was the YOLOv11s object detection model, since in our experiments the accuracy difference between the 's' and 'm' models was not significant, while the speed difference was noticeable.

The FSO CO dataset was used to train the model [13]. This dataset provides over 10,000 annotated images for object detection. These annotation are high quality, since the dataset has quality assurance protocols, unlike the FSO CO Legacy dataset. The FSO CO Legacy contained a high number of very similar images since the teams usually provided images from the same video or the same track. The new FSO CO required that all the candidate dataset must have a low enough similarity score. Also, at least 50% of the candidate data must be on-board footage of rules compliant tracks. The higher quality annotation and the low variability of the images entails a reduced training time.

The dataset was divided between a 70% training set, a 20% validation set and a 10% test set. The model was trained using the training set and the validation set was used to perform a hyperparameter search of the model. After the optimization, the test set was used to

evaluate the overall performance. The best results were obtained at around 40 iterations and further training seemed to cause overfitting. To search the best combination for the 30 hyperparameters a genetic algorithm was used to optimize a fitness function defined as follows:

$$0.1recall + 0.1mAP@0.5 + 0.8mAP@0.5 : 0.95 \quad (1)$$

The genetic algorithm optimized this equation using a mutation of 90% chance and 0.04 variation to create new children of the best parents from previous generations. After the optimization, the model performed a 0.93 mAP@0.5 as it is shown in figure 5.

3) *Object tracker*: A multi object tracker (MOT) is an algorithm that allows recovering the identity information of several detected object across frames [14]. In the presented design an object tracker is used to maintain the cone identities across time. Since the mapping algorithm will also provide a way to identify the cones, there is no need to have a highly precise tracker, therefore it was chosen the Intersection-Over-Union (IOU).

The method assumes that an object detector produces a detection per frame for every object to be tracked. It also assumes that consecutive detections of an object have a high overlap IOU, which is true in sufficiently high frame rates. The IOU measure can be defined using the equation 2.

$$IOU(a,b) = \frac{Area(a) \cap Area(b)}{Area(a) \cup Area(b)} \quad (2)$$

When both requirements are met, tracking with this method can be done without using any image information. The tracker continues the identity by associating the detection with the highest IOU to the last detection in the previous frame if a certain threshold σ_{IOU} is met [15]. All detections not assigned to an existing track will start a new one. All tracks without an assigned detection will end.

4) *Cone positioning*: The 2D positioning is calculated using both the detected images and the depth information. The position was modeled using a distortion-free projective transformation given a pinhole camera model following Equation 3.

$$sp = A[R|t]P_w \quad (3)$$

Where P_w is a 3D point expressed with respect to world coordinates, p is a 2D pixel in the image plane, A is the camera intrinsic matrix, R and t are the rotation and translation that describe the change of world coordinates to camera coordinate systems, and s is the projective transformation's arbitrary scaling and not part of the camera model [16]. The camera intrinsic matrix A is composed of the lengths expressed in pixel units and the principal point following the equation 4.

$$A = \begin{bmatrix} f_x & 0 & c_x \\ 0 & f_y & c_y \\ 0 & 0 & 1 \end{bmatrix} \quad (4)$$

The world coordinates are equal to the camera coordinates since the translation and rotation will be calculated in the mapping node. Therefore, the rotation and translation matrix is the identity $[R|t] = [I|0]$. This model allows to calculate the image projected given the real coordinates. The depth information can be used to calculate the z given the camera intrinsic parameters and the pixel position using similar triangles.

C. Positioning and mapping

The Positioning and Mapping module captures sensor data to determine accurate location and orientation. It consists of the submodules Camera Driver, RTK Driver, Extended Kalman Filter, Mapping, and Map Awareness. RTK and IMU data are the main inputs, which are combined using a Extended Kalman Filter to achieve high accuracy.

The Mapping submodule creates a global map of the circuit by combining location and computer vision data, assigning a linear order to cones and publishing the car's position and map information. Additionally, the map awareness node provides information about the car's position on the track.

1) *Extended Kalman Filter*: A Kalman filter [17] is an algorithm that uses a series of measurements observed over time to produce estimates of unknown variables. The algorithm works in a two-phase process: predict and update. In the prediction phase, the filter estimates the current state variables and uncertainties. In the update phase, these estimates are corrected using a weighted average of the new measurements, prioritizing those with greater certainty.

In the context of autonomous racing, state estimation typically relies on fusing high-frequency ego sensors (IMU, odometry) with positioning systems (GNSS-RTK). For this architecture, we employ the *Kinematic Bicycle Model* as the dynamical system foundation. This model is widely validated in closed circuit racing operations [18] for its optimal balance between computational load and prediction accuracy.

While dynamic models account for complex tire-slip mechanics, the kinematic approach fused with GNSS updates has been proven to maintain decimeter-level accuracy (< 15 cm) in dynamic environments [19]. Furthermore, recent experimental comparisons demonstrate that EKF fusion using this modeling approach can improve localization accuracy by approximately 32% compared to raw sensor data [20], therefore it's selected for achieving the 1-2 cm target accuracy when combined with RTK corrections.

The system control inputs are the longitudinal acceleration a and the steering angle δ , and the measurement outputs are the GNSS coordinates (x, y) , the magnetometer heading angle θ , the vehicle speed v (median of rear wheel speeds), and the IMU angular velocity ω , as shown in Figure 3.

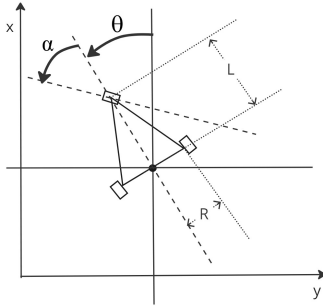


Figure 3. Kinematic Bicycle Model (Tricycle representation)

To model the system, it is required to represent a linear system using a propagation model (equation 5) and a measuring model (equation 6).

$$\vec{x}(k+1) = A\vec{x}(k) + B\vec{u}(k) + \vec{w}(k) \quad (5)$$

$$\vec{y}(k) = C\vec{x}(k) + \vec{v}(k) \quad (6)$$

Where k is the current instant, \vec{x} is the internal state vector, \vec{y} is the input vector, \vec{u} is the output vector, A , B and C are the model matrices, and \vec{v} and \vec{w} are the considered errors. The internal state vector is composed of the x and y coordinates, the turning angle θ and the vehicle speed v .

Our approach used a uniformly accelerated rectilinear motion (UARM) to calculate $x(k+1)$, $y(k+1)$ and $\theta(k+1)$ (equations 7,

8 and 9). And lastly for the speed $v(k+1)$ we simply develop the acceleration formula (equation 10).

$$x(k+1) \simeq x(k) + v_x(k)t_s + \frac{1}{2}accel_x(k)t_s^2 \quad (7)$$

$$y(k+1) \simeq y(k) + v_y(k)t_s + \frac{1}{2}accel_y(k)t_s^2 \quad (8)$$

$$\theta(k+1) \simeq \theta(k) + \dot{\theta}(k)t_s + \frac{1}{2}\ddot{\theta}(k)t_s^2 \quad (9)$$

$$v(k+1) \simeq v(k) + accel(k)t_s \quad (10)$$

Where t_s is the sampling time. With a sampling time small enough, the last component of equations 7, 8 and 9 will be much smaller than the other components, so it can be ignored to simplify the model. In the design, t_s will be 0.1 seconds, because the RTK has a maximum refresh rate of 10Hz. Developing the above equations, the propagation model will follow the equation 11.

$$\begin{bmatrix} x \\ y \\ \theta \\ v \end{bmatrix} (k+1) = \begin{bmatrix} x(k) - t_s v(k) \sin \theta(k) \\ y(k) + t_s v(k) \cos \theta(k) \\ \theta(k) + \frac{t_s}{l} \tan(\alpha(k)) v(k) \\ v(k) + accel(k)t_s \end{bmatrix} \quad (11)$$

- $x(k), y(k)$: Vehicle position coordinates at time step k . These denote the current location of the vehicle in the global (or chosen local) reference frame.
- $\theta(k)$: Heading angle (orientation) of the vehicle at step k , typically in radians.
- $v(k)$: Vehicle's longitudinal velocity (speed) at time k .
- t_s : Sampling interval, i.e., the time difference between steps k and $k+1$ (in seconds).
- $\alpha(k)$: Steering angle at time step k , representing the front wheel's angular deviation from the forward direction.
- l : Wheelbase, that is, the distance between the front and rear axles of the vehicle.
- $accel(k)$: Longitudinal acceleration applied at time k .

Each row of the propagation equation gives the predicted value at the next step ($k+1$), given the current state and applied control input:

- $x(k+1)$: Next x-position, determined by forward motion and heading.
- $y(k+1)$: Next y-position, following a similar principle.
- $\theta(k+1)$: Updated heading angle, proportional to current turning rate.
- $v(k+1)$: Updated speed, incremented by the product of acceleration and sampling time.

$$\begin{bmatrix} x \\ y \\ \theta \\ v \end{bmatrix} (k+1) = \begin{bmatrix} 1 & 0 & 0 & -t_s \sin \theta(k) \\ 0 & 1 & 0 & t_s \cos \theta(k) \\ 0 & 0 & 1 & \frac{t_s}{l} \tan \alpha(k) \\ 0 & 0 & 0 & 1 \end{bmatrix} \begin{bmatrix} x \\ y \\ \theta \\ v \end{bmatrix} (k) + \begin{bmatrix} 0 \\ 0 \\ 0 \\ t_s \end{bmatrix} [accel] + \begin{bmatrix} w_x \\ w_y \\ w_\theta \\ w_v \end{bmatrix} \quad (12)$$

Where \vec{w} is the error. To estimate the error, a normal distribution centered at 0 is assumed, where the covariances are our estimation of the maximum possible error (equation 13). A diagonal covariance

matrix is used since it is assumed that the errors in each internal state are uncorrelated.

$$\begin{bmatrix} w_x \\ w_y \\ w_\theta \\ w_\nu \end{bmatrix} \simeq N(0, Q) \quad Q = \text{Diag} \left(\begin{bmatrix} 0.2^2 \\ 0.2^2 \\ (3 \frac{\pi}{180})^2 \\ (0.5 \frac{1000}{3600})^2 \end{bmatrix} \right) \quad (13)$$

Where $\text{Diag}(\vec{v})$ is a function that returns a square diagonal matrix with the elements of vector \vec{v} on the main diagonal. With equations 12 and 13 the propagation model defined in equation 5 is specified. To specify the measuring model (equation 6), we only need to correlate the internal state with the outputs and add the error, as per equation 14.

$$\mathbf{y}(k) = \begin{bmatrix} x \\ y \\ \theta \\ \nu \\ \omega \end{bmatrix} (k) = \begin{bmatrix} 1 & 0 & 0 & 0 \\ 0 & 1 & 0 & 0 \\ 0 & 0 & 1 & 0 \\ 0 & 0 & 0 & 1 \\ 0 & 0 & 0 & \frac{\tan \alpha}{l} \end{bmatrix} \begin{bmatrix} x \\ y \\ \theta \\ \nu \end{bmatrix} + \begin{bmatrix} v_x \\ v_y \\ v_\theta \\ v_\nu \\ v_\omega \end{bmatrix} \quad (14)$$

Where the \vec{v} error vector is approximated using a normal distribution, mean 0 and covariance the estimated maximum error, following equation 15. In a similar fashion as equation 13 it is assumed that the errors are uncorrelated so a diagonal matrix is used.

$$\begin{bmatrix} v_x \\ v_y \\ v_\theta \\ v_\nu \\ v_\omega \end{bmatrix} \simeq N(0, R) \quad R = \text{Diag} \left(\begin{bmatrix} 0.2^2 \\ 0.2^2 \\ (10 \frac{\pi}{180})^2 \\ (0.5 \frac{1000}{3600})^2 \\ (5 \frac{\pi}{180} \frac{1}{60})^2 \end{bmatrix} \right) \quad (15)$$

Therefore, the model for the Extended Kalman filter is defined using equation 12 with error 13 in the propagation step and equation 14 with error 15 for the measuring step.

2) *Mapping*: The mapping node stores the cone and car positions across time. It uses the first values received by the Extended Kalman Filter as the world reference coordinates. From that point onward, all the coordinate information received will be transformed relative to that reference. The mapping node continuously receives the cone position and identity over time. To avoid the identity switch errors, whenever the mapping node receives a new identity, it checks an oval area across the nearest cone. If the new detection is within this area, it is considered to be the same cone and it updates the new position to a weighted average of all the detections assigned to that cone. To calculate the average, the coefficient is inversely proportional to the distance, so the nearer cones weigh more than the farther ones. This mitigates the error generated by the depth camera previously presented. Since the search area changes inversely proportional with the distance, the nearest cones have a smaller search area than the farther ones. The mapping node publishes the cones currently visible, and all the cones detected so far. These cones must be ordered so the path-planning algorithm works properly. To order the cones it's used a simple algorithm that searches in a triangular area following the vector defined by the previous cone of the same color as represented in figure 4.

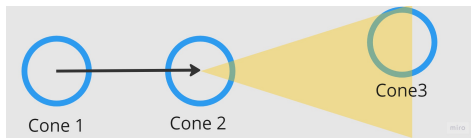


Figure 4. Cone ordering algorithm.

To define the beginning of either side of the track, the algorithm looks for the orange cones indicating the start line that are closest

to the first blue/yellow cones of the track. The triangular search area varies depending on the mission. If several cones are detected in the area, the closest one to the previous cone will be the next counted one. If a detected cone does not fall in any search area, is considered not relevant for this section of the track and will be ignored.

3) *Map Awareness*: The map awareness node uses the mapping and positioning information offered by the mapping node to calculate relevant information about the position of the car in the track. This information differs between missions. The information that this node provides is: the number of laps run, the current kind of lap (recon or timed), whether the finish line has been reached, if the vehicle is near the finish line, and if the vehicle is outside the track limits. In case of the skidpad mission, it also detects when the vehicle is near the skidpad central section, and the number of times it runs across it.

D. Path Planning

The Path Planning node calculates the car's position at each moment, using the Skidpad Filter and Spline submodules. The Spline module calculates the middle point of the track by interpolating the cones, and segments it into points with designated speeds for the Control node to follow.

1) *Spline*: The chosen approach to calculate the racing line is a simple algorithm that follows the middle point of both sides of the track. To calculate the racing line first it's required to define the track constraints. These constraints are defined by interpolating the series of blue and yellow cones respectively. To interpolate the track limits a 2D cubic spline was used. By interpolating individually for the left and right track sides, many imaginary cones can be placed on the track. The chosen approach pairs the imaginary cones on the each side of the track to create transverse lines. Then, the middle point of these transverse lines is calculated and interpolated to obtain the racing line. This racing line is then discretized to obtain the points that the Pure Pursuit must optimize. The path-planning algorithm behaves differently between the discovery and the timed lap. During the discovery lap the spline only uses the currently visible detections. Meanwhile, whenever its detected that the lap is a closed loop, the global path-planning activates and calculates the spline over the whole track [21]. For each point defined by the segmented cubic spline, the node assigns a target speed. This target speed is limited using the maximum allowed speed, the maximum rotation angle and the rotation rate, so the Pure Pursuit can properly follow the path at the defined speeds.

E. Global Map Alignment

For not closed circuit operations, it's necessary to position the ego against the defined track. In this kind of mission, it is insufficient to follow the track definition as it is discovered, specially if the track presents some kind of unusual layout definition (ex. a skidpad track). In this kind of layout, the pathplanning algorithm isn't able to properly calculate a path following the mission rules. To fix these issues, we introduced an alternative pipeline that replaces mapping and pathplanning: Global Map Alignment. In this scenario, the position of the cones is known beforehand, so it's possible to store the position and path of the whole track and load it during the event. The Global Map Alignment node can accurately position the entire track by only seeing the first cones. It achieves this by storing a CSV file containing the position of all cones in the track, and mapping the coordinate frame given by positioning to ground truth using a transformation function, defined as a 2x2 matrix (so we cover rotation and scaling).

When we first detect the orange cones in the beginning of the track, we calculate the transformation function like so:

$$T = \begin{bmatrix} a & b \\ c & d \end{bmatrix} \quad \begin{aligned} g &= x_c y'_c - x'_c y_c \\ a &= \frac{x_t y'_c - x'_c y_t}{g} & b &= \frac{x_c x'_t - x'_c x_t}{g} \\ c &= -\frac{y_c y'_t - y'_c y_t}{g} & d &= \frac{x_c y'_t - x'_c y_t}{g} \end{aligned}$$

Where x_c, y_c are the coordinates of the cones from the vision module; and x_t, y_t are the coordinates of the cones in the CSV track.

This calculation yields T , our transformation function. However, this is just the basic transformation function; it doesn't necessarily transform all cones accurately, particularly because cones located farther from the start zone are highly sensitive to slight changes in the original input. To address this, we iteratively adjust the transformation function by using random numbers, aiming to minimize the following equation:

$$\sum_{i=1}^n \frac{1}{d_i - d_{min} + 1} \quad (16)$$

With d defined as the distance from each cone to its predicted position. The fractional part ensures that cones that are closer are prioritised.

F. Control

The control module moves the vehicle along the calculated path using a Pure Pursuit algorithm. The Pure Pursuit Node calculates the target acceleration, steering and braking based on the path and speed profile from the path planning module, and the current car's position from the mapping module using a geometric following algorithm.

1) *Pure Pursuit Algorithm*: The pure pursuit algorithm works by defining a circular path that intersects with the spline given by path planning. This intersection defines a lookahead point, that is usually 3-5 seconds distance ahead. The acceleration is simpler, and we define the acceleration at any given point as the difference between the current speed and the target speed (defined by the speed profile), multiplied by a constant factor of 0.5 to avoid overshooting. Our implementation is special case of pure pursuit called regulated pure pursuit. This algorithm differs from the general pure pursuit algorithm by having a dynamic lookahead that can be parameterized. This lookahead value is then used in the following equation to determine the delta in steering:

$$\alpha = t - \theta \quad \delta = \text{atan2}(2W * \sin(\alpha), l) \quad (17)$$

Where t is defined as the direction to the target point; θ , as the orientation of the car; δ , as the change in direction needed; W , as the wheelbase of the vehicle; and l as the selected lookahead.

The lookahead is selected following the next equation:

$$l = \max(\min(L_l, |t_v - v|), L_h) \quad (18)$$

Defining L_l and L_h as the lower and higher bounds of the lookahead; and t_v and v as the target speed as defined by the speed profile and the current speed.

G. Master Node

The master node is the system entrypoint. It will manage node activations and the system internal flags. To ensure that the system does not launch any unexpected actuator movements whenever the AS enters the *driving* status, the master node activates the nodes from the path-planning and control packages. When the AS changes the status to any other, these nodes are deactivated.

The master node checks the mission and the internal state variables provided by the VCU via the CAN node, and sets a series of parameters to the other nodes. One of these parameters is the flag to set the initial coordinates and state vectors for the mathematical models.

The master node checks the internal state of each of the nodes that form the AS. If any of these nodes enter an unexpected state, the master node activates the EBS.

IV. RESULTS

The presented architecture was tested both as an end-to-end system, as well as the individual modules performance. Due to hardware accessibility restrictions, the end-to-end system was only tested in simulation, while the individual modules were tested with real world data. To avoid biases, the error distribution observed in the individual sensors during their individual evaluation was replicated in simulation to better reflect the global end-to-end system.

A. Object Detection

As previously mentioned, the object detection model was trained using FSOCO datasets. Split between train, validation and test. After optimizing the hyperparameters using the validation data, the model was evaluated in its classification capabilities using the test data. The results are shown in Figures 5 and 6.

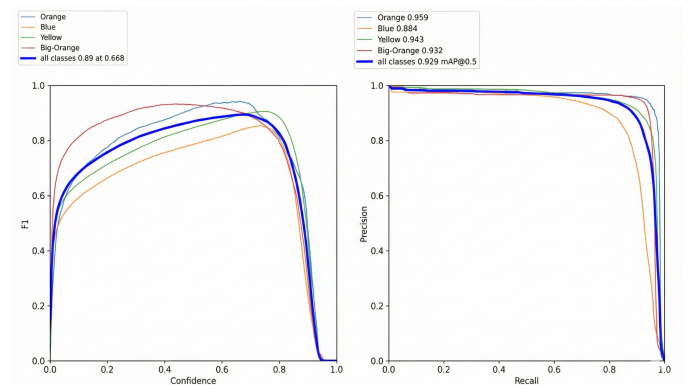


Figure 5. Object detection F1 curve and PR curve.

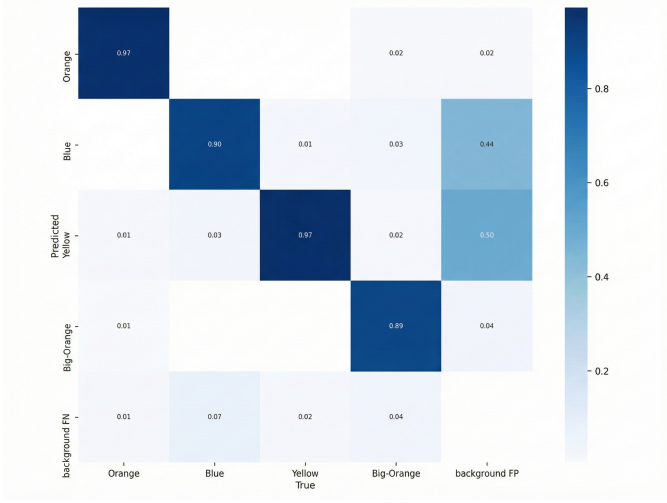


Figure 6. Object detection confusion matrix.

B. Depth calculation

To evaluate the depth calculation algorithms, a real-world testing was done. For this process, the cones that are the detection objectives were located at increasing distances from the camera, and the distance estimation was measured comparatively to the real distance. This test was done at daylight to better evaluate the performance in a real environment. The result of this testing can be seen in Figure 7

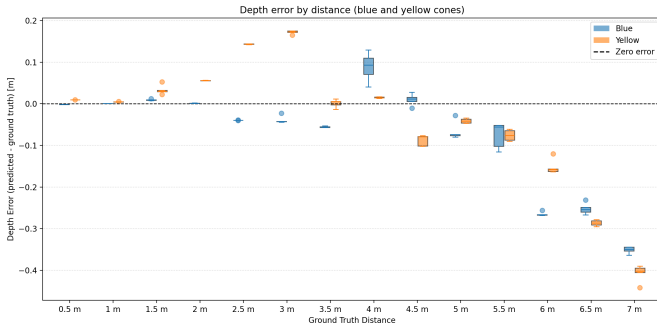


Figure 7. Depth Camera error distribution

As represented in the Figure 7, the error distribution follows an exponential increase, tending to place the objects closer than they actually are as distance increases. It's also noticeable a difference between the estimation of both yellow and blue cones, tending to place the blue cones closer than the yellow ones, specially at medium distances (3m). Overall, for a depth estimation, the error margins in the detection are quite reasonable, since the peak error at 7 meters rounds 50 centimeters. Since the estimation tends to place the objects closer, this approach is "safer" in a real-world environment since the maneuvers will start sooner that is required.

C. RTK data

The RTK data was evaluated comparatively with the GNSS data. This was done via a closed circuit track and measuring both the raw GNSS and the corrected coordinates via RTK. The measurements can be seen in Figures 8 and 9.

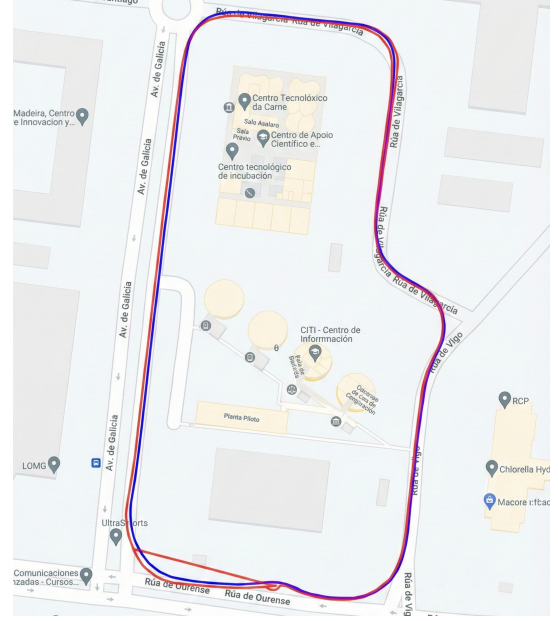


Figure 8. GNSS (Red) vs RTK (Blue) comparative

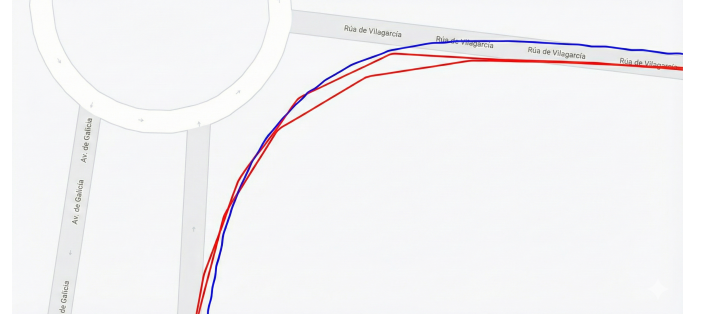


Figure 9. Zoomed in section of the circuit.

As it can be seen, the RTK provides more accurate data, and the loss of signal is more infrequent. These losses of signal in GNSS can be detected in the "straight lines" that are shown on the graph. In the measurements done in this experiments, the precision improved up to a 12 centimeter error using RTK.

D. Car Controls

Finally, to evaluate the car control algorithms, the pipeline is deployed in a simulation environment. In this environment the track is deployed and the perception part of the pipeline is simulated, incorporating the error distribution perceived in the previous experiments. A segment of the circuit is illustrated in figure 10.



Figure 10. Track positioning and error graph.

ACKNOWLEDGMENTS

This project is supported from the Escola Superior de Enxeñaría Informática and Escola Técnica Superior de Enxeñaría Industrial from Universidade de Vigo. Especially with direct help from professors Dr. Miguel Ramón Díaz-Cacho Medina, Dr. Javier Rodeiro Iglesias, Dr. Enrique Paz Domonte and Dr. Joaquín López Fernández.

REFERENCES

- [1] NVIDIA Corporation. *NVIDIA Jetson Orin NX Series: System-on-Module Datasheet*. Version DS-10712-001. Accessed: 2025-12-01. 2023. URL: <https://developer.nvidia.com/embedded/jetson-orin-nx>.
- [2] Steven Macenski et al. “Robot Operating System 2: Design, architecture, and uses in the wild”. In: *Science Robotics* 7.66 (2022), abm6074. DOI: 10.1126/scirobotics.abm6074.
- [3] ArduSimple. *simpleRTK2B – Budget Multiband RTK GNSS Board Data Sheet*. Based on u-blox ZED-F9P module. ArduSimple. 2023. URL: <https://www.ardusimple.com/simplertk2b/>.
- [4] Stereolabs. *ZED 2i: Industrial AI Stereo Camera Datasheet*. Rev. 1.0. 2022. URL: <https://www.stereolabs.com/assets/datasheets/zed-2i-datasheet.pdf>.
- [5] ISO. *ISO 11898-1:2015 – Road vehicles – Controller area network (CAN) – Part 1: Data link layer and physical signalling*. Geneva, Switzerland: International Organization for Standardization, 2015.
- [6] IMechE Formula Student. *FS-AI ADS-DV Software Interface Specification*. Version 4.0. Institution of Mechanical Engineers. 2021. URL: https://github.com/FS-AI/FS-AI_API.
- [7] Open Robotics. *ROS 2 Documentation*. URL: <https://docs.ros.org/en/humble/index.html>.
- [8] StereoLabs. *ZED 2i Camera and SDK Overview*. URL: https://cdn.robotshop.com/rbm/6fadc11e-f9e0-4be9-a52a-4c691a295179/0/035f8ba4-4c7c-4d52-92c8-e62703aedb45/4202a3ed_zed-2i-datasheet.pdf.
- [9] Chien-Yao Wang, Alexey Bochkovskiy, and Hong-Yuan Mark Liao. “YOLOv7: Trainable bag-of-freebies sets new state-of-the-art for real-time object detectors”. In: *arXiv preprint arXiv:2207.02696* (2022).
- [10] Glenn Jocher, Ayush Chaurasia, and Jing Qiu. *Ultralytics YOLOv8*. Version 8.0.0. 2023. URL: <https://github.com/ultralytics/ultralytics>.
- [11] “Ultralytics”. URL: <https://ultralytics.com/>.
- [12] Juan Terven and Diana Cordova-Esparza. “A Comprehensive Review of YOLO: From YOLOv1 to YOLOv8 and Beyond”. In: *arXiv preprint arXiv:2304.00501* (2023).
- [13] Niclas Vödisch, David Dodel, and Michael Schötz. “FSOCO: The Formula Student Objects in Context Dataset”. In: *SAE International Journal of Connected and Automated Vehicles* 5.12-05-01-0003 (2022).
- [14] Wenhao Luo et al. “Multiple object tracking: A literature review”. In: *Artificial intelligence* 293 (2021), p. 103448.
- [15] Erik Bochinski, Volker Eiselein, and Thomas Sikora. “High-Speed tracking-by-detection without using image information”. In: 2017, pp. 1–6. DOI: 10.1109/AVSS.2017.8078516.
- [16] OpenCV. *Camera Calibration and 3D Reconstruction*. URL: https://docs.opencv.org/4.x/d9/d0c/group__calib3d.html.
- [17] Rudolph Emil Kalman. “A New Approach to Linear Filtering and Prediction Problems”. In: *Transactions of the ASME–Journal of Basic Engineering* 82.Series D (1960), pp. 35–45.
- [18] Juraj Kabzan, Miguel Valls, Victor Reijgwart, et al. “AMZ Driverless: The full autonomous racing system”. In: *Journal of Field Robotics* 37.7 (2020), pp. 1267–1294.
- [19] H. Albarakati et al. “Experimental 2D extended Kalman filter sensor fusion for low-cost GNSS/IMU”. In: *Measurement* 200 (2022).
- [20] X. Li, Y. Wang, and H. Zhang. “Adaptive and Robust Kalman Filter-Based Fusion of IMU and UWB for High-Accuracy Localization”. In: *IEEE Sensors Journal* (2025). Demonstrates 32% accuracy improvement using EKF fusion vs raw sensors.
- [21] Adam Slomoi. “Path Planning and Control in an Autonomous Formula Student Vehicle”. PhD thesis. Monash University, 2018.